

PAPER • OPEN ACCESS

Experimental observations of fast-ion losses induced by neoclassical tearing modes in the MAST-U spherical tokamak

To cite this article: J F Rivero-Rodríguez *et al* 2025 *Plasma Phys. Control. Fusion* **67** 045029

View the [article online](#) for updates and enhancements.

You may also like

- [Integrated modelling of tokamak plasmas: progress and challenges towards ITER operation and reactor design](#)
C Bourdelle
- [Semi-analytical model of ion cyclotron resonance heating antenna-plasma coupling and wave propagation in hot magnetized plasma](#)
Claudia Salvia, Alessandro Cardinali, Silvio Ceccuzzi *et al.*
- [STORM modelling of scrape-off layer filament behaviour with hot ions](#)
S Ahmed, J T Omatani, S L Newton *et al.*

Experimental observations of fast-ion losses induced by neoclassical tearing modes in the MAST-U spherical tokamak

J F Rivero-Rodríguez^{1,*} , L Velarde² , T Williams^{1,3} , J Galdón-Quiroga⁴ , M Dreval⁵ , D Dunai⁶ , M García-Muñoz⁴ , K G McClements¹ , J Rueda-Rueda⁷ , E Viezzer⁴ , the MAST Upgrade Team⁸ and the EUROfusion Tokamak Exploitation Team⁹

¹ United Kingdom Atomic Energy Authority, Culham Campus, Abingdon, Oxon OX14 3DB, United Kingdom

² Departamento de Ingeniería Energética, Universidad de Sevilla, Sevilla, Spain

³ Department of Physics and Astronomy, University of Exeter, Stocker Road, Exeter, United Kingdom

⁴ Departamento de Física Atómica, Molecular y Nuclear, Universidad de Sevilla, Sevilla, Spain

⁵ Institute of Plasma Physics, National Science Center, Kharkov Institute of Physics and Technology, 61108 Kharkov, Ukraine

⁶ HUN-REN Centre for Energy Research, Konkoly-Thege út 29-33, 1121 Budapest, Hungary

⁷ University of California at Irvine, Irvine, CA 92697, United States of America

E-mail: juan.rivero-rodriguez@ukaea.uk

Received 11 October 2024, revised 18 February 2025

Accepted for publication 21 March 2025

Published 1 April 2025



CrossMark

Abstract

Neoclassical tearing modes (NTMs) have been identified as the most deleterious perturbations in high-performance plasmas at Mega Amp Spherical Tokamak Upgrade (MAST-U). They produce magnetic islands that flatten the electron temperature profile and enhance the fast-ion transport. Understanding the NTM-induced losses can reveal paths to mitigate them, thus increasing the energy available to heat up the plasma. The MAST-U fast-ion loss detector (FIELD) is equipped with a high-resolution camera and a high-speed camera that simultaneously measure the fast-ion losses in MAST-U. The combination of both systems makes it possible to infer the velocity-space of the losses fluctuating at the frequency of the NTMs. The FILDSIM code is used to infer the velocity space of the fast-ion losses from the strike position in a scintillator plate. Eulerian video magnification is employed to identify the losses that oscillate at the frequencies of the NTMs. NTMs produce fast-ion losses across a broad range of velocity space, with pitch angles ranging from 35° to 54° . Non-linear interactions between the fast-ion orbits and different magnetic islands have been observed. The lost fast-ion orbits meet the stringent conditions that makes it possible to measure these effects.

⁸ See Harrison *et al* 2024 (<https://doi.org/10.1088/1741-4326/ad6011>) for the MAST Upgrade Team.

⁹ See Joffrin *et al* 2024 (<https://doi.org/10.1088/1741-4326/ad2be4>) for the EUROfusion Tokamak Exploitation Team.

* Author to whom any correspondence should be addressed.



Original Content from this work may be used under the terms of the [Creative Commons Attribution 4.0 licence](https://creativecommons.org/licenses/by/4.0/). Any further distribution of this work must maintain attribution to the author(s) and the title of the work, journal citation and DOI.

Keywords: fast particles, fast-ion diagnostics, fast-ion losses, neoclassical tearing modes, spherical tokamak, magnetic confined fusion

1. Introduction

Fusion research is making significant strides towards the achievement of energy production in both magnetically [1] and inertially [2] confined fusion. Spherical tokamaks (STs) are considered a cost-saving route for magnetically confined fusion, as they achieve smaller aspect ratios, $A = R_0/a$, than conventional tokamaks (R_0 and a being the major and minor radii, respectively), but they withstand higher relative pressures, $\beta = \frac{2\mu_0 p}{B^2}$, where μ_0 is the vacuum permeability, p is the plasma pressure and B is the magnetic field. Recent ST experiments have achieved ion temperatures up to 4 keV in Globus-M2 [3] and 8.6 keV in ST40 [4], demonstrating that fusion-relevant ion temperatures can be achieved in STs. The success of any magnetically confined fusion device relies upon good fast-ion confinement, as they provide energy, momentum and current to achieve fusion-relevant plasmas. Fast ions are highly energetic particles so their loss can also endanger the tokamak wall. Even though high-energy charged fusion products are unconfined in present-day STs, fast-ion research in STs is relevant for any burning plasmas, because the fast ions sourced from external heating in STs mimic certain properties of fusion-born α -particles in future devices. Specifically, the fast ion Larmor radii are relatively large (up to 30% the ST minor radius) and they can reach speeds close to or above the Alfvén speed (super-Alfvénic), making it possible to drive unstable a wide variety of magneto-hydro dynamic (MHD) instabilities susceptible to interact with the fast ions [5, 6].

The Mega Amp Spherical Tokamak (MAST) [7] is among the largest STs worldwide ($R_0 = 0.8$ m and $a = 0.5$ m). In 2020, a major upgrade was completed (MAST-U), which expanded its exhaust capabilities, increased the variety of diagnostics and enhanced the overall machine performance [8]. One of the main objectives of MAST-U is to study the fast ions and their interplay with MHD instabilities in deuterium (D) plasmas. MAST-U is equipped with on-axis (south, SS) and off-axis (south–west, SW) neutral beam injectors (NBIs), which are the main source of fast ions and capable of providing up to 5 MW of external heating (up to now, a maximum injected power of 3.5 MW has been achieved). In addition, it is equipped with an extensive array of fast-ion diagnostics, such as the Fast-Ion D- α spectrometer [9]; the neutron camera upgrade [10]; the charged fusion products detector [11], the solid-state neutral particle analyser (SSNPA) [12] and the fast-ion loss detector (FILD) [13, 14]. This suite of diagnostics makes it possible to measure the fast-ion distribution in MAST-U with unique spatial and temporal resolution. Indeed, the MAST-U experiments have provided key information to understand the energetic particle physics in STs, such as experimental evidence of losses due to charge exchange interactions with edge neutrals and the interactions between fast

ions and MHD perturbations like Alfvén eigenmodes, fish-bones and edge localised modes [15].

The MAST-U experiments have revealed the particularly deleterious effect of neoclassical tearing modes (NTMs) in high-performance plasmas [16]. In the last experimental campaign, the peak performance was achieved in the 750 kA plasma current scenario, with $\beta_n = \beta \frac{aB_t}{I_p}$ close to 4 (B_t being the toroidal magnetic field at the magnetic axis and I_p the plasma current). But the performance decreased with the appearance of NTMs (both in β_n and neutron emission, the latter indicating a loss of fast ions). Thus, NTMs affect both the thermal plasma and the fast-ion distribution, as they produce magnetic islands at rational flux surfaces that flatten the electron temperature profile and provide routes for fast-ions to be transported across plasma flux surfaces. The fast-ion transport and losses induced by NTMs have been studied in conventional tokamaks like DIII-D [17], ASDEX Upgrade [18, 19], EAST [20], or HL-2A [21]. Unfortunately, NTMs are ubiquitous in MAST-U high-performance 750 kA plasmas. Thus, to further improve the performance of MAST-U plasmas, the NTMs or, at least, their effect on the plasma need to be mitigated. One way of achieving this is to reduce the loss of fast ions associated with NTMs, as they are the main source of plasma heating in MAST-U. This has motivated studies of the interactions between NTMs and fast ions in this device. Numerical simulations with the MARS-F linear resistive MHD code [22] have revealed a $n = 1$ mode with internal-kink and tearing components in MAST-U 750 kA plasmas, causing losses from a slowing-down fast-ion distribution of over 10% [23]. However, a parametric analysis of the fast-ion velocity space only revealed loss of counter-current orbits, of which there are relatively few in the MAST-U fast-ion distribution, as both beams are injected co-current.

Understanding the velocity-space of the losses is crucial for identifying the phase-space affected by the modes. The FILD makes it possible to experimentally resolve the velocity-space of the fast-ion losses. It works as a magnetic spectrometer, collimating fast-ions that are escaping from the plasma, and recording the light emitted by a scintillator plate when the fast ions impinge on it. Since the strike position is determined by the fast-ions' gyroradii and pitch angles, one can resolve the velocity-space of the losses from the light emitted. The light is recorded by two cameras simultaneously, using a beam splitter. One is a Ximea complementary metal–oxide semiconductor camera that records a high spatial resolution video of the scintillator plate (1 Mpx @ 3500 Hz). This makes it possible to resolve the velocity-space of the losses up to a limited frequency [24]. The other is an APDCAM-10G, consisting of an 8×8 array of avalanche photo-diodes (APDs) that records the fast-ion loss fluctuations with a sampling rate of 4 MHz but a limited resolution in velocity-space. A good

alignment between the cameras makes it possible to combine the two datasets, enabling the study of high-frequency fluctuations in the fast-ion loss velocity-space. This capability will be exploited to infer the velocity-space of fast-ion losses induced by NTMs.

The paper is organised as follows: section 2 provides an overview of the experimental results, revealing non-linear interactions between NTMs and the fast-ion losses. Section 3 provides an analysis of the FILD signal and the use of Eulerian video magnification (EVM) to identify the fast-ion loss velocity-space oscillating at the frequencies of the NTMs. Section 4 traces the fast-ion orbits measured by the FILD and discusses the interaction between those orbits and the NTMs. Finally, section 5 provides a summary and a discussion of the results.

2. Experimental observations

The NTM-induced fast-ion losses are investigated in MAST-U shot #46943, a 750 kA plasma in H-mode regime with $B_t = 0.54$ T at the magnetic axis ($R_{\text{axis}} = 1.0$ m) and conventional double-null divertor. The main plasma parameters are shown in figure 1. The plasma is heated by both SS and SW NBIs. The distance between the FILD head and the separatrix is 7 cm. Characteristically for MAST-U, the line-integrated density rises linearly throughout the H-mode phase of the discharge from $6 \cdot 10^{-19}$ m $^{-2}$ to $37 \cdot 10^{-19}$ m $^{-2}$. The MAST-U outboard Mirnov array for high frequency data acquisition (OMAHA) coils [25] detects magnetic instabilities in the plasma, as shown in figure 1(f). A mode with a constant frequency around 8 kHz can be observed during most of the flat-top. Between $t = 0.3$ s and $t = 0.4$ s, a mode that starts at 38 kHz rapidly sweeps down in frequency to 22 kHz at which point it disappears. The toroidal mode numbers, n , can be determined by the phase difference between toroidally separated OMAHA coils, and by this means we have found that the 8 kHz mode has $n = 1$ and the 38 kHz mode has $n = 2$. The dominant poloidal mode number of the 8 kHz mode has been determined to be $m = 2$ using soft x-ray measurements, but the dominant m of the 38 kHz could not be determined experimentally. However, the frequencies of the modes are equal to the plasma rotation frequencies at rational flux surfaces $q = 2$ and $q = 1.5$, respectively, multiplied by their toroidal mode number. Thus, the 8 kHz mode is identified as an $(m, n) = (2, 1)$ NTM, localised at the $q = 2$ rational flux surface, while the mode starting at 38 kHz is a $(3, 2)$ NTM, localised at the $q = 1.5$ rational flux surface.

Note that another kind of rotating MHD mode is also observed in MAST-U plasmas, known as long-lived mode [26]. These are ideal saturated kink modes driven unstable as the safety factor approaches unity, with regions of negative or low magnetic shear. However, in pulse #46943, $q_{\text{min}} > 1.35$ and the plasma does not show any region of reverse magnetic shear. Thus, the observed modes are most likely NTMs.

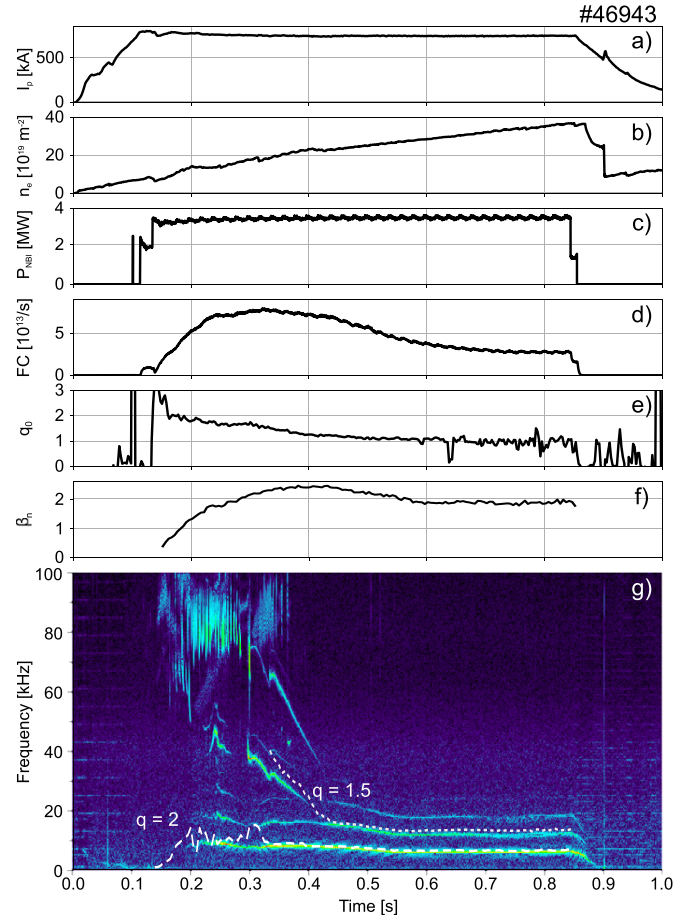


Figure 1. From top to bottom, plasma current, line-integrated density, total NBI power, neutron emission measured from a fission chamber, plasma safety factor in the core, β_n and OMAHA coil spectrogram in MAST-U pulse #46943. The white dashed lines mark the plasma rotation frequency multiplied by the n of the respective island.

The NTMs produce magnetic islands with the indicated poloidal and toroidal periodicity, which typically flattens the electron temperature profile around the rational flux surfaces where they are localised. This flattening is observed by Thomson scattering to be 6 cm wide for the $(2, 1)$ NTM and 5 cm for the $(3, 2)$ NTM, as shown in figure 2. Both modes show harmonics at higher toroidal mode numbers, labelled in figure 3(a).

Figure 3 shows a close-up comparison of the OMAHA and FILD spectrograms, during the time period when the two NTMs coexist. The FILD spectrogram, which represents the oscillation frequency of the detected fast-ion losses, reveal frequencies above 50 kHz that are not detected by the OMAHA coils or a CO $_2$ interferometer which also has a sampling rate that is high enough to detect fluctuations in this range. These frequencies are equal to the sum of the individual NTM frequencies or their harmonics, indicating a non-linear interaction between the fast-ion orbits and the NTMs. Two waves with different frequencies, ω_1 and ω_2 , propagating in the same

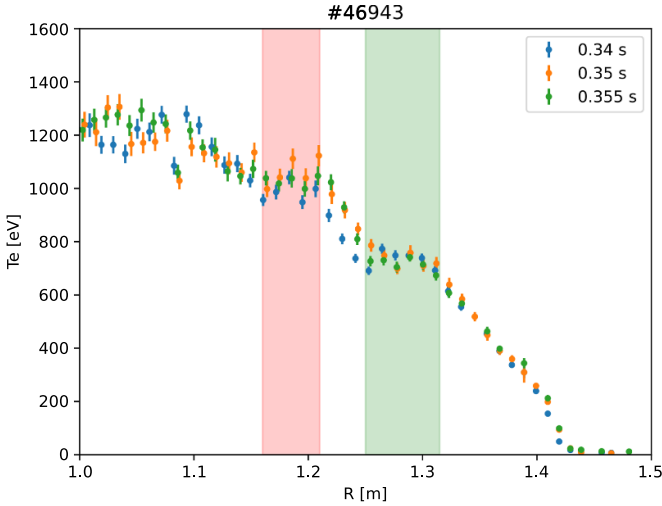


Figure 2. Electron temperature measured by Thomson scattering. The flattening caused by the (3,2) and the (2,1) magnetic island is shaded in red and green, respectively.

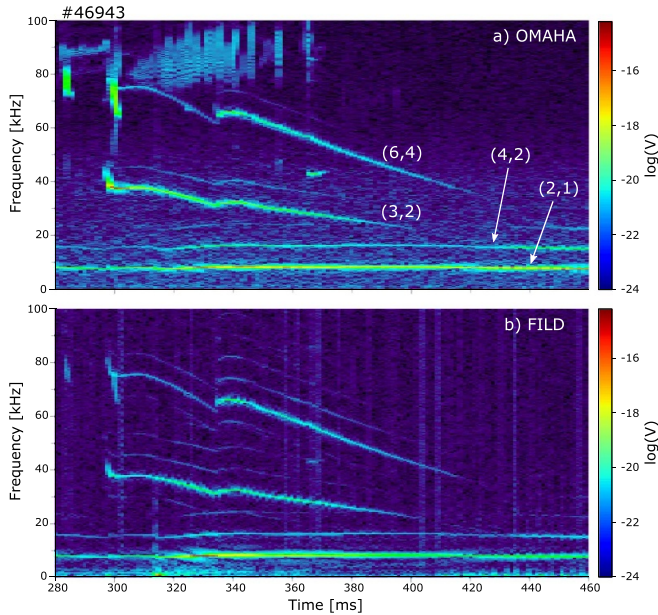


Figure 3. Spectrogram of (a) OMAHA coil and (b) FILD APD channel [3,5] in MAST-U shot #46943.

medium can non-linearly interact with each other, resulting in waves at the sum and difference frequencies $\omega = \omega_1 \pm \omega_2$. Similarly, fast-ion orbits can non-linearly interact with different perturbations in the plasma, even if the modes do not interact with each other. The fast ions orbital response couples with one mode as the ion passes through it, affecting the wave-particle phase when the ions traverse the following wave, producing fast-ion losses at the sum and difference frequency of the modes fundamental frequencies. This effect was observed in DIII-D with reversed shear Alfvén eigenmodes, and toroidal Alfvén eigenmodes [27, 28]. A simple uniform-plasma analytic theory predicted that the non-linear interaction between

fast-ions and modes produce peaks where the amplitude of the difference frequency is always larger than the sum frequency [27], and this is clearly not the case here, as the observed frequencies are above the frequencies of both modes. Heidbrink *et al* [28] showed that, experimentally, peaks at the sum frequency higher than peaks at the difference frequency can be observed, as there are four conditions that must be met in order to observe peaks in the FILD spectrum:

- (i) There are orbits that are resonant with the wave.
- (ii) The orbits intersect the mode spatially.
- (iii) The orbits pass close to FILD.
- (iv) The NBI populates these orbits.

In the following sections, we will aim to identify the fast-ion orbits that meet these conditions and therefore are susceptible to non-linearly interact with the NTMs.

3. Velocity-space analysis of NTM-induced losses

In this section we will be analysing the velocity-space of the losses in shot #46943. Figure 4 shows the fast-ion losses measured by the Ximea camera at $t = 0.36$ s. The FILD strike map is computed with the FILDSIM code [29], which calculates the velocity-space that corresponds to each point of the scintillator plate, using the equilibrium reconstructed by EFIT++. This makes it possible to remap the losses into gyroradius ($\rho_L = \frac{mv}{|q|B}$) and pitch-angle ($\Lambda = -\arccos v_{\parallel}/v$), as shown in figure 5. Here, m and q are the mass and charge of the ion, and v , v_{\perp} and v_{\parallel} are the total, perpendicular and parallel velocity of the fast ion with respect to the magnetic field, B . Four distinct fast-ion loss distributions can be observed, with pitch angles 35° , 42° , 47° and 54° . Considering that the finite dimension of the diagnostic collimator distorts mono-energetic distributions across the gyroradius direction [24], each of these distributions can be assumed mono-energetic. The gyroradii at the FILD probe of the injection energy of the SW (73 keV) and SS (60 keV) NBIs correspond to 13.2 cm and 12.4 cm, respectively, which are marked in figure 5. Thus, the peaks of the 3 distributions between $\Lambda = [30^{\circ}, 50^{\circ}]$ are at $\rho_L = 13.2$ cm, close to the injection energy of the SW NBI. On the other hand, the peak of the 54° distribution is at 11.9 cm, which is close to the injection energy of the SS NBI. Therefore, it can be assumed that the distributions at 35° , 42° and 47° are sourced from the SW NBI, while the distribution at 54° from the SS NBI. This is confirmed by comparing the time of appearance of each distribution with the start time of their respective NBI. In the following, the energy of the losses will be assumed that of their respective NBI injection energy.

As previously mentioned, the sampling rate of the Ximea camera limits our ability to resolve the velocity-space of losses induced by modes with frequencies above half the sampling frequency of that camera. In shot #46943, the sampling frequency was 1 kHz. Therefore, to solve the velocity-space of the fast-ion losses fluctuating at the frequency of the NTMs, the data of the Ximea and the APDCAM must be combined.

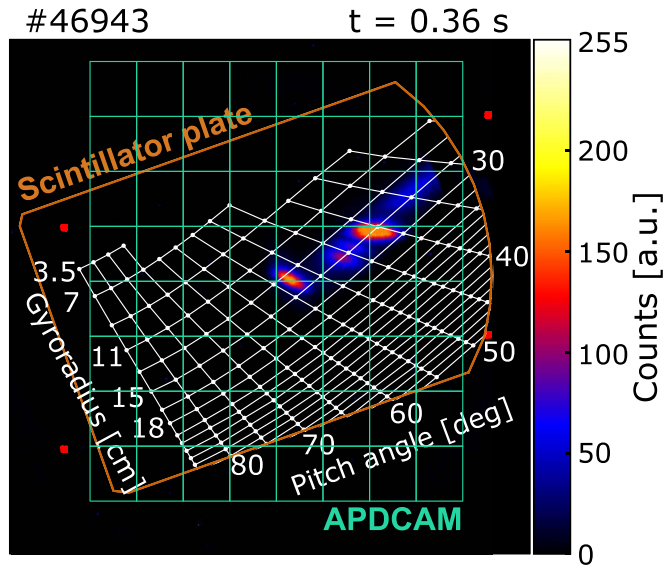


Figure 4. Frame of the Ximea camera in MAST-U shot #46943 at $t = 0.36$ s. The contour of the scintillator plate is marked in orange. The FILDSIM strike map is shown in white. The field of view of the APDCAM sensor is shown in green. In red are the ends of the optical fibres surrounding the APDCAM sensors that enable the alignment of the cameras.

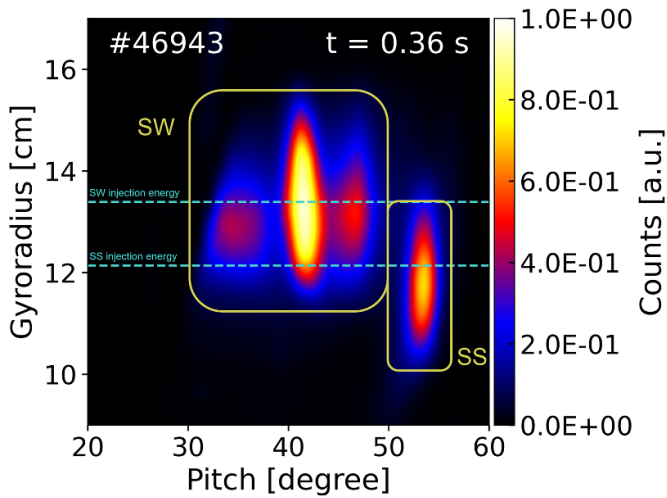


Figure 5. Velocity-space of the fast-ion losses measured by FILD in MAST-U shot #46943 at $t = 0.36$ s. Reproduced from [15]. The Author(s). [CC BY 4.0](https://creativecommons.org/licenses/by/4.0/).

To do so, the cameras must be aligned so that the field of view of one camera can be correlated with the other. The APDCAM includes 4 fibre optics whose ends (red dots in figure 4) surround the APDCAM sensor (in light green). These fibres can be lit up, creating 4 spots of light at the APDCAM sensor plane. This light travels through the FILD optical system, producing a focused image of the 4 spots on the scintillator plate. These spots of light on the scintillator plate can be recorded by the Ximea camera, thus making it possible to align both fields of view, as show in figure 4. The APDCAM frame at $t = 0.36$ s is shown in figure 6(a). This frame shows the light

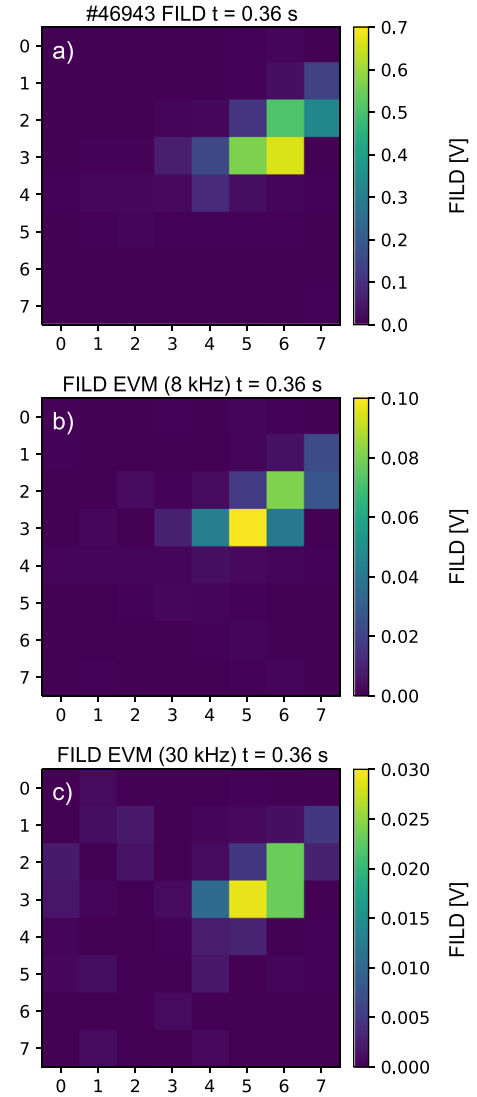


Figure 6. (a) APD frame of MAST-U shot #46943 at $t = 0.36$ s. (b) The same APD frame processed with EVM using a bandpass filter of [6.5, 9.0] kHz and (c) a bandpass filter of [27.0, 31.0] kHz.

intensity measured by each APD, which is equivalent to the Ximea frame in figure 4. Thus, following the nomenclature $[i,j]$ to identify individual APDs, where i is the APD row and j is the APD column, we can observe that the 35° distribution is recorded by [1,7], [2,7] and [2,6]; the 42° distribution is recorded by [2,6], [2,5], [3,6] and [3,5]; the 47° distribution by [3,5] and the 54° distribution by [3,3], [3,4] and [4,4]. The APDCAM frame in figure 6(a) is a coarse representation of the Ximea frame in figure 4, confirming the alignment of the cameras.

But figure 6(a) does not provide any additional information in comparison to figure 4. Thus, to highlight fluctuations in the APDCAM data caused specifically by the presence of the NTMs we use EVM [30]. EVM is a numerical tool that applies spatial decomposition, followed by temporal filtering, to reveal subtle oscillations in videos. It has been previously used to observe the structure of MHD modes in

MAST with a fast visible camera [31]. By applying EVM to the APDCAM data we are able to highlight the specific regions of the velocity-space affected by the presence of the NTMs. Figure 6(b) shows the EVM-processed APDCAM data with a bandpass filter of [6.5, 9.0] kHz, thus highlighting the oscillations of the (2,1) NTM. The results show a wide light pattern similar to figure 6(a), indicating that the (2,1) NTM is expelling losses across a broad range of velocity space. EVM also reveals a phase shift of $0.11T$ (being T the period of the (2,1) NTM) between the oscillations in APD [3,5] and [2,7]. This indicates that different phases of the (2,1) NTM—i.e. different poloidal and toroidal positions of the magnetic islands—can induce losses with a very different velocity-space (pitch angles from 35° to 47°). In contrast to the raw frame, the maximum amplitude of the EVM-processed frame is at APD [3,5]. This likely corresponds to the distribution (73 keV, 47°), revealing a strong interaction between those orbits and the (2,1) NTM. The EVM output that highlights the oscillations of the (3,2) NTM (using a bandpass filter of [27.0, 31.0] kHz) is shown in figure 6(c). In this case, the oscillation is more concentrated between APDs [3,4], [3,5], [3,6] and [2,6], with amplitudes 3 times lower than the 8 kHz oscillations. This shows a weaker interaction and more localised in velocity-space between the losses and the (3,2) NTM. Since both EVM-processed frames have their maxima in [3,5], the most plausible lost orbit to non-linearly interact with both NTMs is the (73 keV, 47°).

4. Fast-ion orbits interacting with NTMs

In this section we are going to analyse whether the orbits of the measured fast-ion losses overlap with the NTMs identified in the MAST-U plasma, and thus that they are susceptible to interact with the magnetic islands. Figure 7 shows the lost fast-ion orbits in #46943 at $t = 0.36$ s, tracked with the ASCOT5 Monte-Carlo full-orbit code [32]. The equilibrium is reconstructed with EFIT++, constrained with the motional Stark effect (MSE) diagnostic. MSE measures the magnetic field pitch across the midplane, thus achieving a more accurate reconstruction of the q profile. The $q = 2$ and $q = 1.5$ rational flux surfaces are highlighted in green and red, respectively. The width of the islands estimated with Thomson scattering are shaded in their respective colours. The orbits of fast ions with pitch angles 35° , 47° and 54° and energies 73 keV, 73 keV and 60 keV respectively at the FILD are shown in the figure. The 42° orbit is not shown to improve clarity, but it is an intermediate passing orbit between the orbits with pitch angles 35° and 47° .

The particle tracking shows that all the orbits overlap with the $q = 2$ rational flux surface, confirming the interaction of the (2,1) NTM with a broad range of fast-ion loss velocity-space. The 35° orbit does not intersect the (3, 2) NTM. Therefore, this orbit cannot interact with the (3,2) NTM. On the other hand, orbits with pitch angles 47° and 54° overlap with the (3,2) NTM, while the 42° orbit is very close to overlapping.

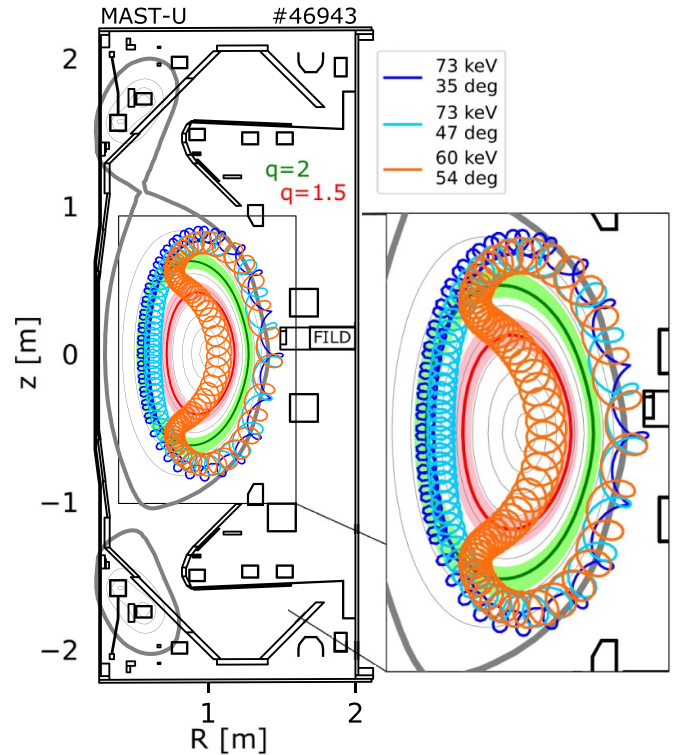


Figure 7. Fast-ion loss orbits (73 keV, 35°), (73 keV, 47°) and (60 keV, 54°) tracked with ASCOT5 in the MSE-constrained equilibrium of MAST-U shot #46943 at $t = 0.36$ s. The $q = 2$ and the $q = 1.5$ rational flux surfaces are marked in green and red, respectively.

This indicates that only orbits with $\Lambda > 42^\circ$ are susceptible to interact with both islands.

If we compare these conclusions with the EVM-processed data, we observe that indeed, the full velocity-space range of lost fast ions oscillates at the frequency of the (2,1) NTM, confirming the interaction of a broad range of lost fast ions with this mode. The highest oscillations at the frequency of the (3,2) NTM correspond to the APD channels of the 47° pitch-angle, whose orbit overlaps both islands. Therefore, both the EVM analysis and the ASCOT5 particle tracking indicate that the 47° pitch angle orbit is the best candidate to non-linearly interact with both NTMs.

5. Conclusions

NTMs are considered one of the most deleterious MHD perturbations in MAST-U, limiting the plasma performance in current experiments. One of the consequences of NTMs is the loss of fast ions that limits the available energy to heat up the bulk plasma. TRANSP/NUBEAM simulations estimate a total loss of 17% of the confined fast-ion population [15], which is in the order of the 20% lost beam power due to orbital losses and charge exchange losses [33]. Thus, understanding the fast-ion losses induced by NTMs becomes key to improving the plasma performance in MAST-U.

This paper solves experimentally the velocity-space of the fast-ion losses induced by NTMs in MAST-U. To achieve that, the data of the two cameras in the MAST-U FILD (Ximea and APD) are combined to identify the fast-ion losses with high temporal and velocity-space resolution. FILDSIM solves the velocity-space of the losses measured with the Ximea camera, while EVM is used to highlight fluctuations in the APDCAM data at the frequencies of the NTMs. The FILD detects a wide range of fast-ion losses interacting with the (2,1) NTM, with pitch angles ranging from 35° to 54° . In the case of the (3,2) NTM, only losses above $\Lambda > 42^\circ$ interact with it. Particle tracking confirms these observations: while all lost orbits overlap the (2,1) island, the lost orbits with $\Lambda \leq 42^\circ$ do not overlap the (3,2) island, due to its innermost location, explaining why they do not interact with it.

The FILD measurements have revealed a non-linear interaction between the fast-ion losses and the NTMs when the fast-ion orbits traverse several magnetic islands. The observation shows the sensitivity of the diagnostic to this non-linear interaction. However, given the 4 restrictive conditions in which these experimental observations are made (see section 2), non-linear interactions of fast ions with MHD perturbations are likely to be more frequent than observed. On the other hand, there are many cases in MAST-U in which modes of the same amplitude coexist but non-linear peaks are not observed. The ASCOT simulations only indicate the plausibility of the non-linear interaction between the 47° pitch-angle orbit and the magnetic islands because the orbit overlaps the two islands. To confirm this interaction, particle tracking simulations must include the magnetic perturbation induced by the NTMs [21], which is left for future work.

The (2,1) NTM, ubiquitous in high-performance MAST-U plasmas, interacts with a broad range of fast-ion velocity-space, even at different phases. According to this, it seems unlikely that one can tweak the fast-ion distribution to avoid these losses while the (2,1) NTM is present. The (3,2) NTM does not cause as many fast-ion losses, due to its innermost location, but it could be causing fast-ion redistribution that might not be captured by FILD. For this reason, in the current experimental campaign (2024–2025), dedicated experiments are developing NTM-free scenarios with the aim to increase the plasma performance. Transient suppression of the NTMs has been achieved by upshifting the plasma, which will make it possible to compare the fast-ion losses with and without NTMs in future experiments. In future campaigns, an absolute calibration of FILD will make it possible to provide absolute measurements of the NTM-induced fast-ion losses.

Data availability statement

The data cannot be made publicly available upon publication because they are not available in a format that is sufficiently accessible or reusable by other researchers. The data that support the findings of this study are available upon reasonable request from the authors.

Acknowledgment

The authors would like to thank Dr Christopher Ham for his insightful help identifying some of the modes described in this paper.

This work has been carried out within the framework of the EUROfusion Consortium, funded by the European Union via the Euratom Research and Training Programme (Grant Agreement No. 101052200 — EUROfusion) and from the EPSRC (Grant Number EP/W006839/1). To obtain further information on the data and models underlying this paper please contact PublicationsManager@ukaea.uk. Views and opinions expressed are however those of the author(s) only and do not necessarily reflect those of the European Union or the European Commission. Neither the European Union nor the European Commission can be held responsible for them.

This project has received funding from the European Research Council (ERC) under the European Union's Horizon 2020 research and innovation programme (Grant Agreement No. 805162).

The simulations were partly performed on the MARCONI supercomputer (CINECA).

J. Galdon-Quiroga acknowledges support from the MSCA PF programme under Grant No. 101069021.

ORCID iDs

J F Rivero-Rodríguez  <https://orcid.org/0000-0001-5074-0267>

L Velarde  <https://orcid.org/0000-0002-3986-1583>

J Galdón-Quiroga  <https://orcid.org/0000-0002-7415-1894>

M Dreval  <https://orcid.org/0000-0003-0482-0981>

M García-Muñoz  <https://orcid.org/0000-0002-3241-502X>

K G McClements  <https://orcid.org/0000-0002-5162-509X>

J Rueda-Rueda  <https://orcid.org/0000-0002-4535-326X>

E Viezzer  <https://orcid.org/0000-0001-6419-6848>

References

- [1] Mailloux J *et al* 2022 *Nucl. Fusion* **62** 042026
- [2] Abu-Shawareb H *et al* 2022 *Phys. Rev. Lett.* **129** 075001
- [3] Kurskiev G *et al* 2024 *Phys. Plasmas* **31** 062511
- [4] McNamara S *et al* 2023 *Nucl. Fusion* **63** 054002
- [5] Sharapov S E *et al* 2014 *Phys. Plasmas* **21** 082501
- [6] Bakharev N *et al* 2023 *Phys. Plasmas* **30** 072507
- [7] Cox M 1999 *Fusion Eng. Des.* **46** 397–404
- [8] Harrison J R *et al* 2019 *Nucl. Fusion* **59** 112011
- [9] Michael C A *et al* 2013 *Plasma Phys. Control. Fusion* **55** 095007
- [10] Ceconello M *et al* 2023 *Plasma Phys. Control. Fusion* **65** 035013
- [11] Perez R V *et al* 2014 *Rev. Sci. Instrum.* **85** 11D701
- [12] Prechel G *et al* 2022 *Rev. Sci. Instrum.* **93** 113517
- [13] Rivero-Rodríguez J F *et al* 2018 *Rev. Sci. Instrum.* **89** 10I112
- [14] Rivero-Rodríguez J F *et al* 2024 *IEEE Trans. Plasma Sci.* **52** 3878–3884
- [15] Rivero-Rodríguez J F *et al* 2024 *Nucl. Fusion* **64** 086025
- [16] Harrison J R *et al* 2024 *Nucl. Fusion* **64** 112017
- [17] Forest C *et al* 1997 *Phys. Rev. Lett.* **79** 427
- [18] García-Muñoz M *et al* 2007 *Nucl. Fusion* **47** L10

- [19] Galdon-Quiroga J et al 2018 *Nucl. Fusion* **58** 036005
- [20] Yu L et al 2021 *AIP Adv.* **11** 025020
- [21] Zhang Y, Wang F, Sun J, Li M and Hao G 2024 *Plasma Phys. Control. Fusion* **66** 085014
- [22] Liu Y et al 2000 *Phys. Plasmas* **7** 3681
- [23] Liu Y et al 2024 *Plasma Phys. Control. Fusion* **67** 035016
- [24] Velarde L et al 2024 *Plasma Phys. Control. Fusion* **67** 015024
- [25] Hole M et al 2009 *Rev. Sci. Instrum.* **80** 123507
- [26] Chapman I et al 2010 *Nucl. Fusion* **50** 045007
- [27] Chen X et al 2014 *Nucl. Fusion* **54** 083005
- [28] Heidbrink W W et al 2016 *Phys. Plasmas* **23** 022503
- [29] Galdon-Quiroga J et al 2018 *Plasma Phys. Control. Fusion* **60** 105005
- [30] Wu H-Y, Rubinstein M, Shih E, Gutttag J, Durand F and Freeman W 2012 *ACM Trans. Graph.* **31** 1–8 Proc. SIGGRAPH 2012
- [31] Ham C and Harrison J 2022 *2nd Technical Meeting on Plasma Disruptions and their Mitigation* (available at: <https://conferences.iaea.org/event/281/contributions/24423>)
- [32] Hirvijoki E et al 2014 *Comput. Phys. Commun.* **185** 1310–21
- [33] Ollus P et al 2024 *Plasma Phys. Control. Fusion* **66** 025009